Control Technique for the Operation of Grid-Tied Converters with High Penetration of Renewable Energy Resources

Majid Mehrasa [a], Edris Pouresmaeil [b,*], Amir Sepehr [b], Bahram Pournazarian [b], Mousa Marzband [c], and João P. S. Catalão [a,d,e,*]

[a] C-MAST, University of Beira Interior, 6201-001 Covilhã, Portugal
[b] Department of Electrical Engineering and Automation, Aalto University, 02150 Espoo, Finland
[c] Faculty of Engineering and Environment, Department of Physics and Electrical Engineering, Northumbria University Newcastle, Newcastle, UK
[d] INESC TEC and the Faculty of Engineering of the University of Porto, 4200-465 Porto, Portugal
[e] INESC-ID, Instituto Superior Técnico, University of Lisbon, 1049-001 Lisbon, Portugal

***Abstract*—**This paper deals with a control technique based on inherent characteristics of synchronous generators (SG) for control of interfaced converters with high penetration of renewable energy resources (RERs) into the power grid, as a new contribution to earlier studies. To present an appropriate assessment of the proposed control technique, under dynamic operating condition, a P-Q curve is extracted and analysed based on the different components and characteristics of the interfaced converter as well as the conventional relationship between the active and reactive power. By combining the swing equation of SG and the power-based dynamic model, a P_m-Q curve is achieved and the effects of the variations of embedded virtual inertia on virtual mechanical power are assessed. Moreover, by using small-signal linearization, the grid frequency stability is investigated based on both virtual inertia and mechanical power variations. In order to assess the power sharing ability of the proposed control technique, two transfer functions are obtained and then, the impacts of variations of virtual mechanical power on the active and reactive power of interfaced converter are evaluated through Nyquist and Root Locus diagrams. Simulation results confirm that the proposed control technique can guarantee the operation of interfaced converters, based on inherent characteristics of SG, to deal with the power grid stability with high penetration of RERs.

***Index Terms*—**Renewable Energy Resources; Synchronous Generator; Power Grid Stability; Virtual Inertia; Virtual Mechanical Power Error.

* Corresponding authors: Edris Pouresmaeil (edris.pouresmaeil@gmail.com) and João P. S. Catalão (catalao@ubi.pt).

I. Nomenclature

Parameters	
R	Resistance of Grid Interfaced Converter
L	Inductance of Grid Interfaced Converter
C	DC-Link Capacitor
J	Virtual Inertia
k_{pp} & k_{pq}	Proportional Coefficients of Control Components
k_{ip} & k_{iq}	Integral Coefficients of Control Components
ω_{12}	Angular Frequencies of Low Pass Filter
α_{12}	Control Factor of Active Power
β_{12}	Control Factor of Reactive Power
Abbreviations	
RERs	Renewable Energy Resources
DSC	Double Synchronous Controller
PMSG	Permanent Magnet Synchronous Generator
VMPE	Virtual Mechanical Power Error
VI	Virtual Inertia
LPF	Low Pass Filter
PCC	Point of Common Coupling
Variables	
i_{dq}	Interfaced Converter Currents
v_{dq}	Voltages of PCC
v_{dc}	DC Link Voltage of Interfaced Converter
u_{dq}	Switching Functions of Interfaced Converter
i_{dc}	DC Link Current of Interfaced Converter
P	Active Power of Interfaced Converter
Q	Reactive Power of Interfaced Converter
P_{c1}	Power of DC link current and d-Component Voltage
P_{c2}	Power of DC link current and q-Component Voltage
P_{pd}	Power due to d-Component Voltage
P_{pdq}	Power due to d and q-Component Voltage
P_m	Virtual Mechanical Power
ω	Angular Frequency
ΔP	Active Power Error
ΔQ	Reactive Power Error
ΔP_m	Virtual Mechanical Power Error
$\Delta\omega$	Angular Frequency Error
P^*	Reference Value of Active Power
Q^*	Reference Value of Reactive Power
P_m^*	Reference Value of Virtual Mechanical Power
ω^*	Reference Value of Angular Frequency

II. Introduction

Integration of large-scale renewable energy resources (RERs) into the power grid offers several benefits i.e., economic and environmental issues. Meantime, it also raises different technical challenges regarding the grid stability and reliability due to the high variability, unpredictable fluctuation and intermittent characteristic of these sources [1-2]. Generally, RERs are connected to the power grid via power electronics converters, which the lack of inertia in these converter-based power generators, besides their peculiar transient dynamics behaviour, increase their negative impacts on the power grid stability, just the opposite of the operation of synchronous generators (SGs). Consequently, the operation of converter-based generators should be controlled with some specific functionalities based on inherent characteristics of SGs; thus, successfully reaching their high penetration level in the power grid. Therefore, designing an appropriate control technique for control of interfaced converters to deal with the stability issues of power grid has been regarded as one of the main tasks between scientists in power and energy societies [3-4].

Various control targets such as the accurate power sharing and grid voltage regulation have been considered in a large-scale integration of microgrid or multi-distributed generations (DG) connections for achieving a stable performance [5-6].

In addition, along with revealing the challenges of high penetration of RERs into the power grid [7-8], several control strategies have focused on improving the stability of grid frequency and voltage magnitude. For this reason, several studies have been reported in the literature regarding the emulation of SGs characteristics by power converters [9]-[19].

Reference [9] has presented a complete review associated with the main concepts of virtual SGs and their ability at controlling the power grid with the high level of DGs penetration. A coordinated control-based energy storage system combined with virtual SGs has been proposed in [10] to provide emulation of SG for power converters. Numerical simulations have been used in [11] to illustrate a specific virtual synchronous machine-based concept along with its related mathematics for controlling power converters in smart grid application. A generic model has been proposed for a two-stage grid-connected PV system that is able to provide both droop-based response and inertia emulation and a linearized small-signal model for evaluating stability of the proposed PV power control loop [12]. As it has been known that the lack of inertia leads to deteriorating the operation of traditional grid-connected current control with high penetration of RERs, reference [13] has investigated the dynamics abilities of the droop control and virtual synchronous generator (VSG) by the use of small-signal models and finally an inertial droop control strategy has been proposed based on this comparison.

In the way of emulating the inertia of SGs [14], reference [15] has proposed a control technique based on a generic inertia emulation scheme to provide stable operation for multi-terminal voltage-source-converter (VSC)-based high voltage direct current (HVDC) systems. Based on a virtual inertia (VI) control, performance of the PMSG has been compared with a doubly fed induction generator-based wind power system in [16] and also two control strategies based on the dynamic and adaptive fuzzy-based schemes have been proposed. In reference [17], the inertia constant, DERs frequency droop coefficient and the load frequency controllers' parameters have been modelled as a multi-objective optimization and finally solved by multi-objective optimization algorithm. To develop SG-based controllers [18], reference [19] has designed a synchronverter-based control technique for HVDC application.

This paper firstly proposes a dynamic model based on the active and reactive power of the interfaced converter. Then, the proposed model is used to be combined with the SG swing equations for designing a control technique based on emulated behaviours of SG in power grid.

In fact, the proposed control technique presents a new model of power electronics-based SG to guarantee a stable operating condition for the power grid with high penetration of RERs, which is the main contribution of this work over the other existing works in this area.

This paper is organized as the following steps. The power-based dynamic model, the proposed SG-based control technique, and the P-Q curve and its related discussions are presented in section III. The P_m-Q curve is presented in sub-section IV. A. Also, evaluation of the grid frequency variations based on virtual inertia, virtual mechanical power, and interfaced converter specifications is given in sub-section IV. B. In section V, the effects of virtual mechanical power error on the active and reactive power of the interfaced converter are assessed. Simulation results are discussed in detail in section VI and conclusion is given in section VII.

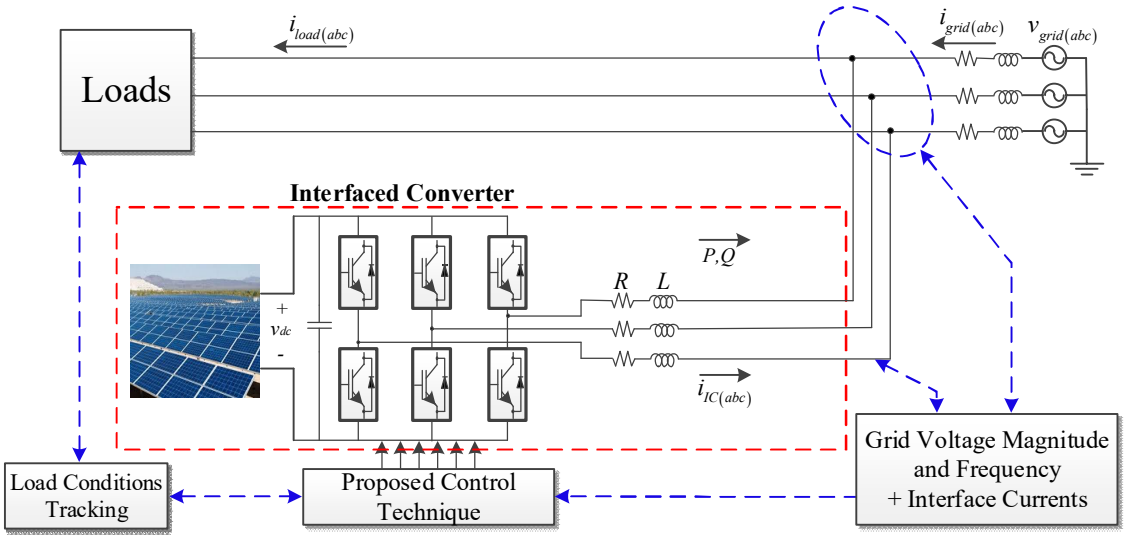

Fig. 1. General structure of the proposed Model.

III. Presentation of the Proposed Control Strategy

It is assumed that the negative effects of high penetration of RERs should be damped by the proposed control-based converter depicted in Fig. 1. Firstly, the basic dynamic equation of the grid-connected interfaced converter can be written as [6]:

$$L\frac{di_d}{dt} + Ri_d - \omega L i_q - u_d v_{dc} + v_d = 0 \quad (1)$$

$$L\frac{di_q}{dt} + Ri_q + \omega L i_d - u_q v_{dc} + v_q = 0$$

$$C\frac{dv_{dc}}{dt} + u_d i_d + u_q i_q + i_{dc} = 0$$

According to (1), the proposed dynamic model is based on the active and reactive power of the interfaced converter. As it is known, the relationship between the interfaced converter currents and power can be stated as:

$$P=i_d v_d \tag{2}$$

$$Q=-i_q v_d \tag{3}$$

By substituting (2) and (3) into (1) and some simplifications, a new dynamic model can be achieved as:

$$\frac{L}{R}\frac{dP}{dt}+P+\frac{\omega L}{R}Q-u_d P_{c1}+P_d=0 \tag{4}$$

$$\frac{L}{R}\frac{dQ}{dt}+Q-\frac{\omega L}{R}P+u_q P_{c1}-P_{dq}=0 \tag{5}$$

$$RC\frac{dP_{c1}}{dt}+u_d P-u_q Q+P_{c2}=0 \tag{6}$$

where, $P_{c1}=v_{dc}v_d/R$, $P_{c2}=i_{dc}v_d$, $P_d=v_d^2/R$, and $P_{dq}=v_d v_q/R$. Equations (4)-(6) demonstrate the power-based dynamic model of the interfaced converter shown in Fig. 1 in which the active and reactive power are the main state variables that should be appropriately controlled. By achieving the switching functions of u_d and u_q from (4) and (5) respectively and substituting the achieved results in (6), the equation for the P-Q curve of the interfaced converter can be obtained as:

$$\left(P+\frac{\frac{L}{R}P_{av}+P_d}{2}\right)^2+\left(Q+\frac{\frac{L}{R}Q_{av}-P_{dq}}{2}\right)^2= \tag{7}$$

$$\left(\frac{\frac{L}{R}P_{av}+P_d}{2}\right)^2+\left(\frac{\frac{L}{R}Q_{av}-P_{dq}}{2}\right)^2-RCP_{c1av}P_{c1}-P_{c2}P_{c1}$$

Fig. 2 illustrates the P-Q curve given in (7). As can be seen from Fig.2, increasing P_d leads to the larger values for the radius and one centre component of the P-Q curve depicted as spotted light blue. In contrast, the simultaneous increment of P_d and P_{dq} can generate a bigger P-Q curve; so that, the coordinates of its centre will be transferred as shown in spotted red colour. It can be noticed that the ability of the interfaced converter will be significantly improved for various active and reactive power generation with bigger radius and centre coordinates.

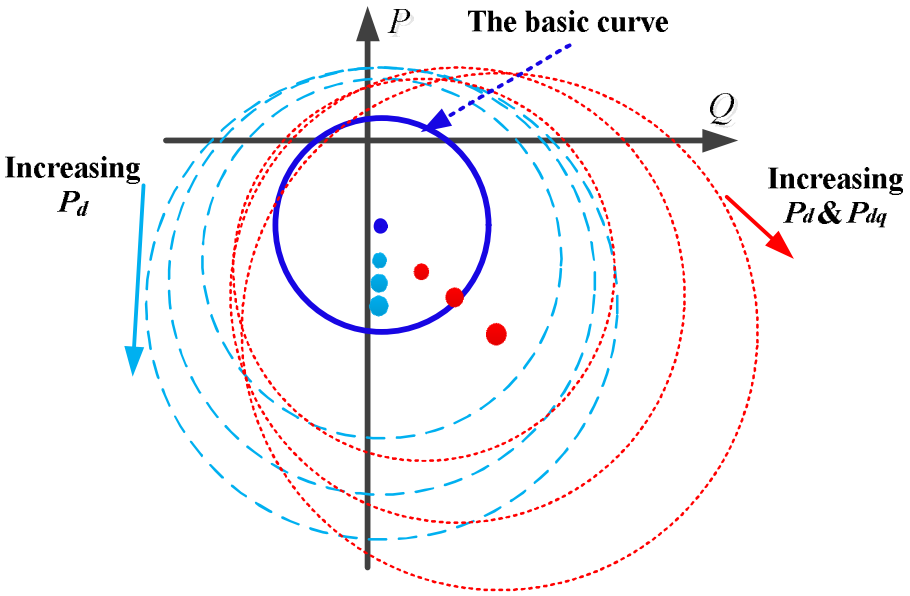

Fig. 2. P-Q curve of the interfaced converter.

A. Presentation of the Proposed SG-based Control Technique

To provide a control technique with the characteristics of SG for control of interfaced converter, the main features of SG should be included in the dynamic equations of the interfaced converter. At first step, the swing equation of PMSG is considered as:

$$J\frac{d\omega}{dt}=\frac{P_m-P}{\omega} \tag{8}$$

In order to involve the inertia and mechanical power of (8) in the control loop of interfaced converter, the small signal method should be applied to (8) as:

$$\Delta\omega=\frac{1}{\omega^* J}\cdot\frac{\Delta P_m-\Delta P}{s+\left(P_m^*-P^*\right)/\omega^{*2}J} \tag{9}$$

By the use of (9), an appropriate and updated value for reaching the reference value of frequency has been achieved for both components of the proposed control technique as shown in Fig.3. In order to reach a control technique based on a suitable operation of virtual inertia and mechanical power, (9) can be rewritten as:

$$\frac{\Delta P}{s}=\frac{\Delta P_m}{s}-\left(\omega^* J+\frac{\left(P_m^*-P^*\right)}{\omega^* s}\right)\Delta\omega \tag{10}$$

For a constant apparent power of the interfaced converter, the following relation can be achieved as:

$$P^2+Q^2=S^2=constant \tag{11}$$

The small signal method is applied to (11) and the result can be placed in (10) to obtain the following relationship:

$$\frac{\Delta Q}{s} = -\frac{P^*}{Q^*}\frac{\Delta P_m}{s} + \frac{P^*}{Q^*}\left(\omega^* J + \frac{\left(P_m^* - P^*\right)}{\omega^* s}\right)\Delta\omega \tag{12}$$

It can be understood from (10) and (12) that, a good response for the active and reactive power of the interfaced converter can be obtained by a zero value for the VMPE, and appropriate values for the P_m^* and for the J, to reach a minimum value of angular frequency error. Thus, by considering the equations (4)-(6), (10), and (12), the closed-loop descriptions of the proposed control technique can be achieved as depicted in Fig. 3. Noticing the equations of (10) and (12), the PI controller coefficients employed in Fig.3 can be stated as,

$$k_{pp} = \omega^* J, \quad k_{ip} = \frac{P_m^* - P^*}{\omega^*} \tag{13}$$

$$k_{pq} = \omega^* J P^* / Q^*, k_{iq} = \frac{\left(P_m^* - P^*\right)P^*}{\omega^* Q^*}$$

As can be seen from Fig.3, all virtual inertia, the reference value of virtual mechanical power and VMPE can impact on the active and reactive power of the interfaced converter that are investigated in section V. By combining (7) and (11), the following linear relationship can be achieved between the active and reactive power injected through the interfaced converter:

$$P = \frac{\left(P_{dq} - \frac{L}{R}Q_{av}\right)}{\left(\frac{L}{R}P_{av} + P_d\right)}Q - \frac{RCP_{c1av}P_{c1} + P_{c2}P_{c1} + S^2}{\left(\frac{L}{R}P_{av} + P_d\right)} \tag{14}$$

In fact, (14) is a linear relationship that shows the active and reactive power near to the desired operating conditions. Principle of this linear relation is drawn in Fig. 4. Increasing P_{dq} and decreasing P_d will lead to a noticeable decrement for the reactive power as shown in Fig. 4. It shows that the zero reactive power can be achieved by increasing the ramp of the linear relation (14). On the other hand, by decreasing P_{dq} and increasing $P_{d,}$ the active power will approach to the following value:

$$P = -\frac{RCP_{c1av}P_{c1} + P_{c2}P_{c1} + S^2}{\left(\frac{L}{R}P_{av} + P_d\right)} \tag{15}$$

According to (15), as P_d increases, the zero active power will be finally obtained. Also, by regulating P_{c1} and P_{c2}, more effective control can be provided for the active power. The aforementioned discussions about (14) can be concluded that the grid voltage magnitude regulation employed in P_{dq}, P_d, P_{c1}, and P_{c2} has a main role at an accurate active and reactive power sharing.

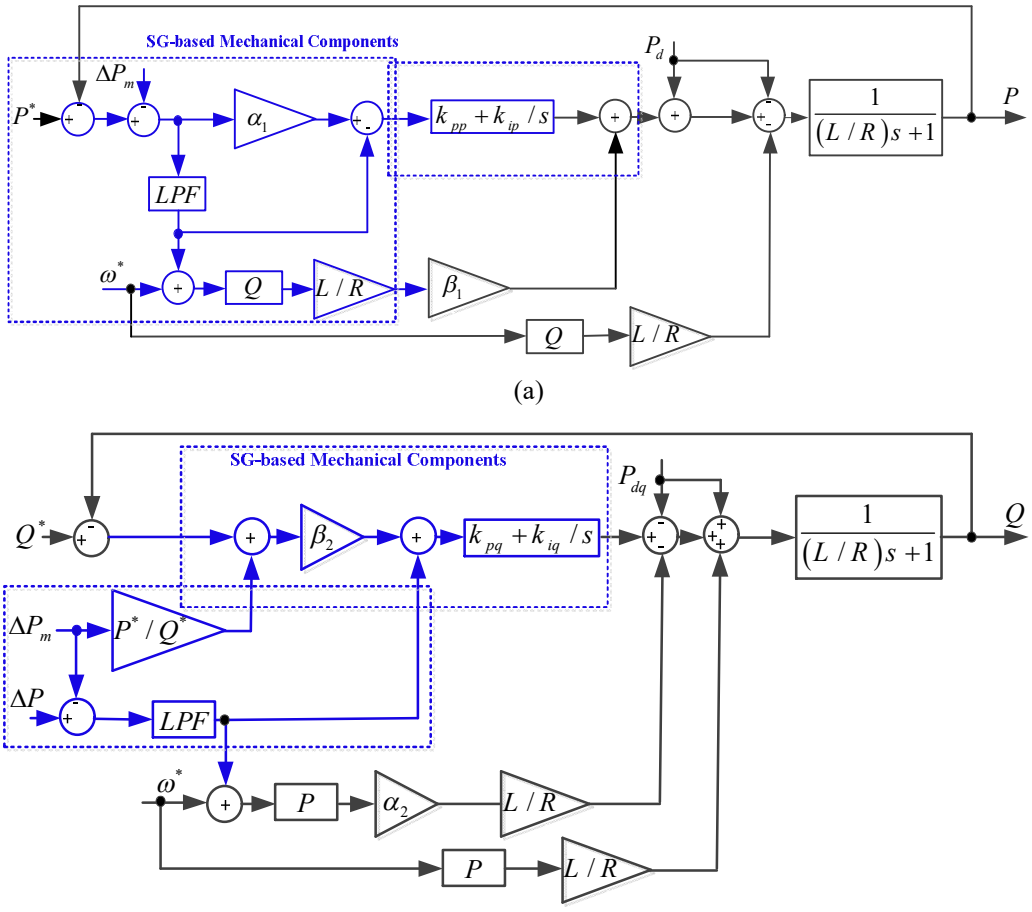

Fig. 3. Closed loops description of the proposed control technique: (a) the active power, and (b) the reactive power.

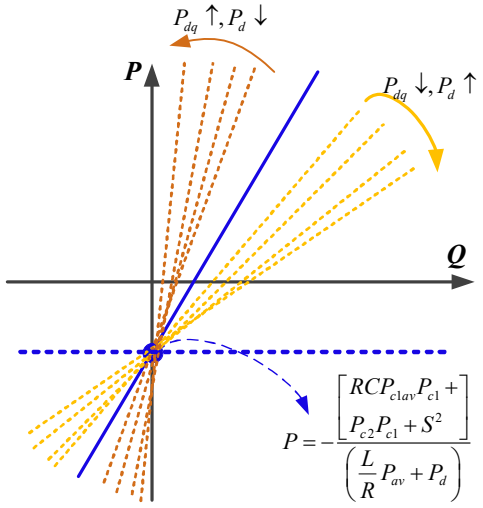

Fig. 4. Linear relation between the active and reactive power of interfaced converter.

IV. Evaluation of the Proposed P_m-Q Curve and Grid Frequency Variation

More analysis associated with both the proposed dynamic model and control technique are accomplished in this section based on introducing a virtual mechanical power-based new curve as well as the effective factors relating to the variations of angular frequency error.

A. Assessment of the Proposed Curve P_m-Q

In order to achieve the new P_m-Q curve, the swing equation in (8) should be incorporated with (7) that consequently the following new curve based on the virtual mechanical power can be driven as:

$$\left(P_m+\left[\frac{\frac{L}{R}P_{av}+P_d}{2}-\omega J\frac{d\omega}{dt}\right]\right)^2+\left(Q+\frac{\frac{L}{R}Q_{av}-P_{dq}}{2}\right)^2= \left(\frac{\frac{L}{R}P_{av}+P_d}{2}\right)^2+\left(\frac{\frac{L}{R}Q_{av}-P_{dq}}{2}\right)^2-RCP_{c1av}P_{c1}-P_{c2}P_{c1} \tag{16}$$

The curve of (16) is drawn in Fig. 5. As can be seen, increasing the virtual inertia can make more shifts to up in comparison with the grid angular frequency increment. It causes the proposed control technique to have more positive values for its virtual mechanical power in various operating conditions. Moreover, it can be understood form Fig. 5(c), the simultaneous increment of ω and *J* can provide bigger positives values for VMP; however, variation of ω is not suitable for performance of the proposed control technique. Thus, the best option is to increase value of inertia *J* in such limited level so that acceptable VMP should be achieved for operation of the proposed control technique. On the other hand, Fig. 5 verifies that the embedded VMP variations can affect operation of the interfaced converter.

B. Assessment of the Grid Frequency Variations

The small signal method is applied to (4) and subsequently (17) can be obtained as:

$$\left(\frac{L}{R}s+1\right)\Delta P+\frac{\Delta\omega L}{R}Q^*+\frac{\omega^* L}{R}\Delta Q-\Delta u_d P_{c1}^*-u_d^*\Delta P_{c1}+\Delta P_d=0 \tag{17}$$

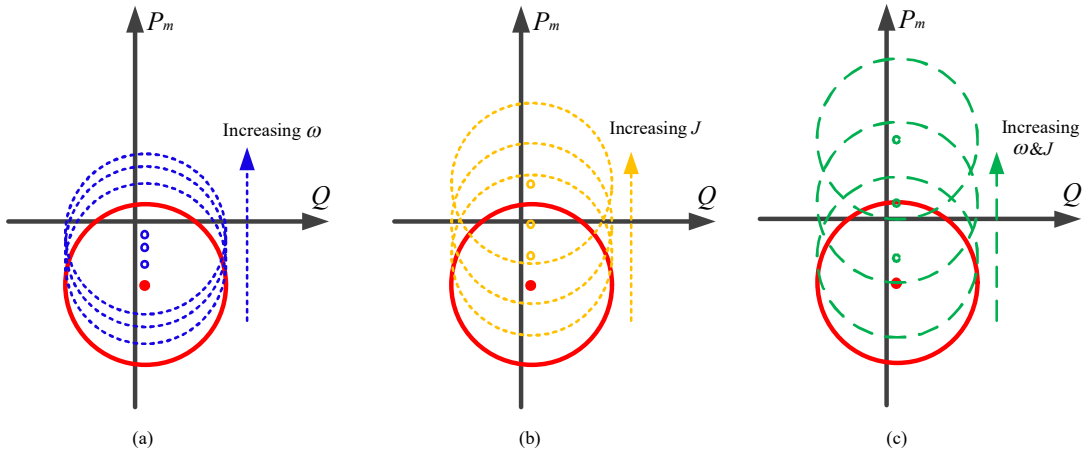

Fig. 5. P_m-Q Curve, (a) increasing ω, (b) increasing J, and (c) increasing ω and J.

By achieving ΔP from (9) and substituting the result into (17), variations of the grid frequency can be achieved as:

$$\Delta\omega = F_{P_m}\Delta P_m + F_Q\Delta Q + F_{u_d}\Delta u_d + F_{P_{c1}}\Delta P_{c1} + F_{P_d}\Delta P_d \tag{18}$$

where,

$$F_{P_m} = \frac{\left(\frac{L}{R}s+1\right)}{\Delta_\omega}, F_Q = \frac{\frac{\omega^* L}{R}}{\Delta_\omega}, F_{u_d} = -\frac{P_{c1}^*}{\Delta_\omega}, F_{P_{c1}} = -\frac{u_d^*}{\Delta_\omega}, F_{P_d} = \frac{1}{\Delta_\omega} \tag{19}$$

$$\Delta_\omega = \left(\frac{\omega^* JL}{R}s^2 + \left[\left(\frac{\left(P_m^* - P^*\right)L}{R\omega^*}\right) + \omega^* J\right]s + \left[\left(P_m^* - P^*\right)/\omega^* + \frac{Q^* L}{R}\right]\right)$$

Based on (18), the effects of each component are considered to evaluate the responses of the grid angular frequency versus the different values of virtual inertia. As can be seen from (18) and (19), the transfer function related to the VMPE is different from other components errors. For three virtual inertia values of $J_3>J_2>J_1$, the Nyquist diagrams of transfer functions around the operating angular frequency associated with the VMPE and other errors are drawn in Fig. 6. As can be seen in Figs. 6(a) and (b), increasing the virtual inertia leads to better response for the grid angular frequency error in the presence of various error components. In fact, increasing the virtual inertia can help the proposed control technique to reach a grid frequency near to its reference value with almost zero error.

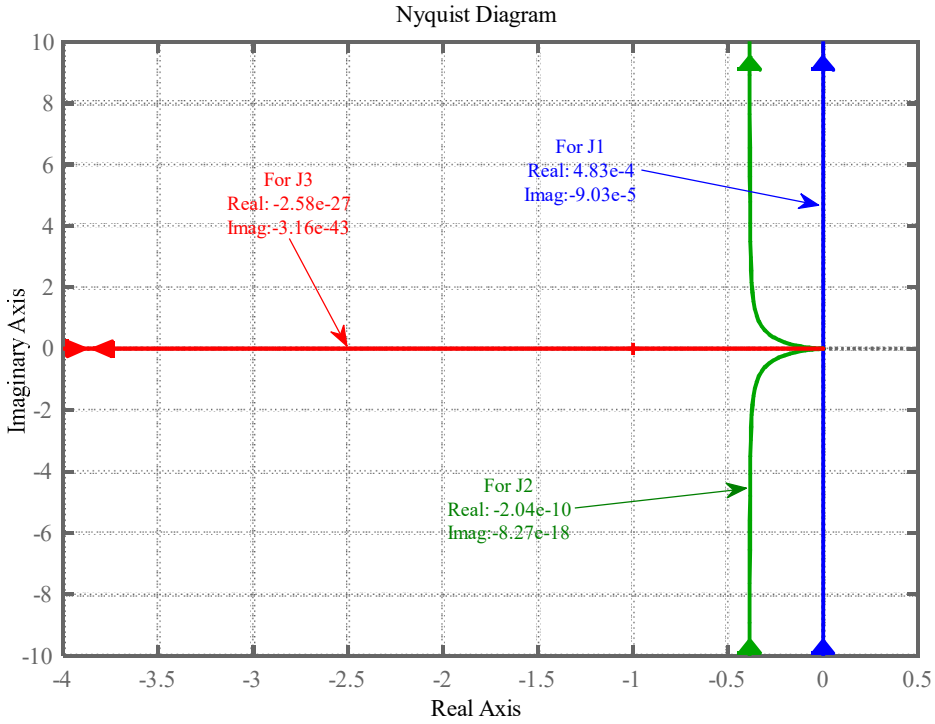

(a)

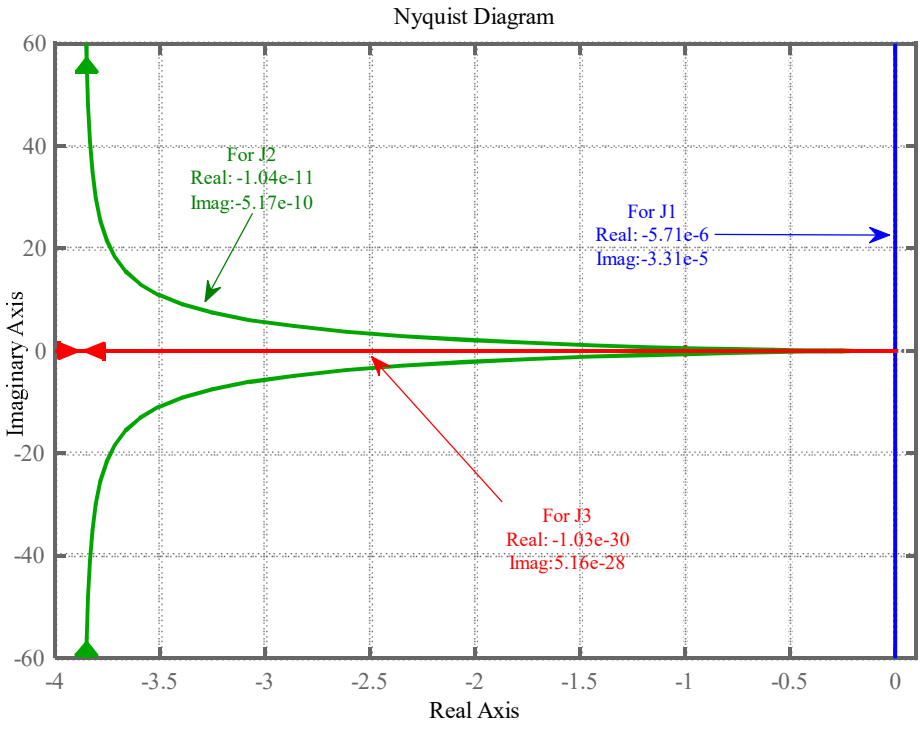

(b)

Fig. 6. The Nyquist diagram of Δω versus the step variation of: (a) VMPE (ΔP_m), and (b) other components errors of (ΔQ, Δu_d, ΔP_{c1}, and ΔP_d).

V. Impacts of Virtual Mechanical Power Errors on the Active and Reactive Power Sharing

Performance of the proposed control technique can be affected by variations of VMPE in which the various values of virtual inertia have its own effects. Thus, the active and reactive power sharing of the proposed control technique should be assessed in this condition. Considering the active and reactive power as well as VMPE in Fig. 2, two following transfer functions are achieved as:

$$\frac{P}{\Delta P_m} = -\frac{\left(\begin{array}{l} k_{pp}\alpha_1\left(L/R\right)s^4 + \left[\left(1+\beta_2 k_{pq}\right)k_{pp}\alpha_1 + \left(L/R\right)\left(k_{ip}\alpha_1 + k_{pp}\omega_2\alpha_1\right) - \left(L/R\right)\omega_1 k_{pp}\right]s^3 \\ + \left[\begin{array}{l}\beta_2 k_{iq}k_{pp}\alpha_1 + \left(1+\beta_2 k_{pq}\right)\left(k_{ip}\alpha_1 + k_{pp}\omega_2\alpha_1\right) + \\ \left(L/R\right)k_{ip}\omega_2\alpha_1 + \beta_2\omega_1 Q^*\left(L/R\right)\beta_1 k_{pq} - \left(1+\beta_2 k_{pq}\right)\omega_1 k_{pp} - \left(L/R\right)k_{ip}\omega_1\end{array}\right]s^2 \\ + \left[\begin{array}{l}\beta_2 k_{iq}\left(k_{ip}\alpha_1 + k_{pp}\omega_2\alpha_1\right) + \left(1+\beta_2 k_{pq}\right)k_{ip}\omega_2\alpha_1 \\ +\beta_2\omega_1 Q^*\left(L/R\right)\beta_1 k_{iq} - \beta_2 k_{iq}k_{pp}\omega_1 - \left(1+\beta_2 k_{pq}\right)k_{ip}\omega_1\end{array}\right]s + \beta_2 k_{iq}k_{ip}\omega_2\alpha_1 - k_{ip}\beta_2 k_{iq}\omega_1 \end{array}\right)}{\left(\begin{array}{l} \left(L/R\right)^2 s^5 + \left(\left(1+\beta_2 k_{pq}\right)\left(L/R\right) + \left(L/R\right)\left(1+\left(L/R\right)\omega_2\right) + \left(L/R\right)k_{pp}\alpha_1\right)s^4 \\ + \left[\begin{array}{l}\beta_2 k_{iq}\left(L/R\right) + \left(1+\beta_2 k_{pq}\right)\left(1+\left(L/R\right)\omega_2\right) + \left(L/R\right)\omega_2 + \left(1+\beta_2 k_{pq}\right)k_{pp}\alpha_1 + \\ \left(L/R\right)\left(k_{ip}\alpha_1 + k_{pp}\alpha_1\omega_2\right) - \left(L/R\right)\omega_1 k_{pp}\end{array}\right]s^3 \\ + \left[\begin{array}{l}\beta_2 k_{iq}\left(1+\left(L/R\right)\omega_2\right) + \left(1+\beta_2 k_{pq}\right)\omega_2 + \beta_2 k_{iq}k_{pp}\alpha_1 + \\ \left(1+\beta_2 k_{pq}\right)\left(k_{ip}\alpha_1 + k_{pp}\alpha_1\omega_2\right) + \left(L/R\right)k_{ip}\alpha_1\omega_2 + \beta_2\omega_1 Q^*\left(L/R\right)\beta_1 k_{pq} \\ -\left(1+\beta_2 k_{pq}\right)\omega_1 k_{pp} - \left(L/R\right)\omega_1 k_{ip}\end{array}\right]s^2 \\ + \left[\begin{array}{l}\beta_2 k_{iq}\omega_2 + \beta_2 k_{iq}\left(k_{ip}\alpha_1 + k_{pp}\alpha_1\omega_2\right) + \\ \left(1+\beta_2 k_{pq}\right)k_{ip}\alpha_1\omega_2 + \beta_2\omega_1 Q^*\left(L/R\right)\beta_1 k_{iq} - \\ \beta_2 k_{iq}k_{pp}\omega_1 - \left(1+\beta_2 k_{pq}\right)\omega_1 k_{ip}\end{array}\right]s + \beta_2 k_{iq}k_{ip}\alpha_1\omega_2 - \beta_2 k_{iq}\omega_1 k_{ip} \end{array}\right)} \tag{20}$$

$$Q/\Delta P_m = A_m/\Delta \tag{21}$$

Fig. 7 shows the impacts of the variations of VMPE on the proposed control technique in the active power sharing. Based on Fig. 7(a), the magnitude of active power for both step and ramp changes of the VMPE are very low. This shows that a VMPE with high magnitude can enforce the proposed control technique to produce an additional term for active power. As can be understood from Fig. 7(b), the step change of VMPE cannot lead to an unstable response from the active power of the proposed control technique. On the other hand, the ramp variation of VMPE can cause the proposed control technique to generate a fluctuated active power as shown in the Root Locus diagram in Fig. 7(c). The step and ramp changes of VMPE lead to a low magnitude of the reactive power that has a little larger magnitude compare with active power as depicted in Fig. 8(a). According to Fig. 8(b) and Fig. 8(c), the step and ramp VMPE generates stable and oscillating responses for reactive power, respectively.

Totally, it results in zero or low magnitude of VMPE, the proposed control technique cannot be affected by variations of VMPE and consequently an accurate and stable performance of active and reactive power sharing are obtained in this condition.

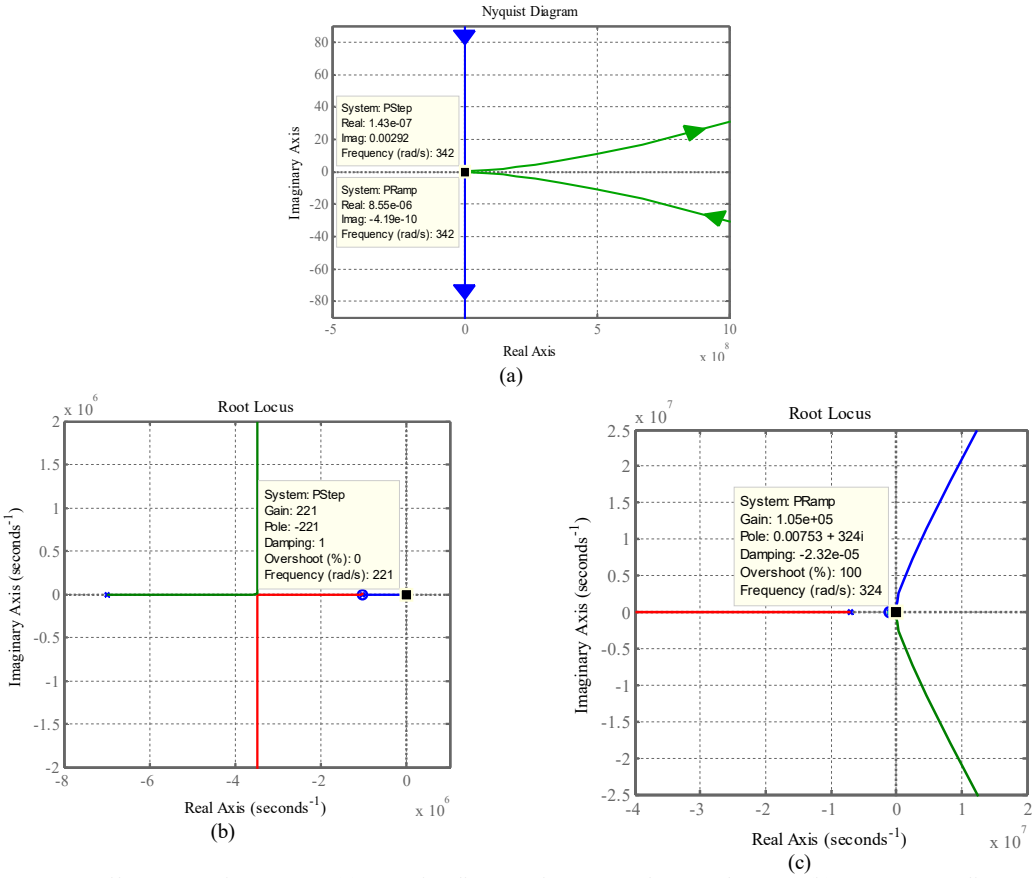

Fig. 7. VMPE effects on active power: (a) Nyquist diagram for step and ramp changes, (b) Root Locus diagram for step change, and (c) Root Locus diagram for ramp change.

VI. Results and Discussions

Abilities of the proposed control technique are assessed in this section by MATLAB/Simulink. In the first evaluation, both steady and dynamic operations of the proposed control technique are considered by load variation. Then, the effects of changing VMPE and VI will be discussed based on the grid frequency and voltage magnitude with high penetration of RERs. Simulation parameters are given in Table I. General structure of the proposed control technique is shown in Fig. 9.

TABLE I: SIMULATION PARAMETERS

Parameter	Value	Parameter	Value
dc-link Voltage (v_{dc})	850 V	J	1e3 s
Phase ac voltage	220 V	Pm	3.3 kW
Fundamental frequency	50 Hz	P	3 kW
Switching frequency	10 kHz	Q	2 kVar
Interface converter resistance	0.1 Ohm	Interface converter inductance	45 mH

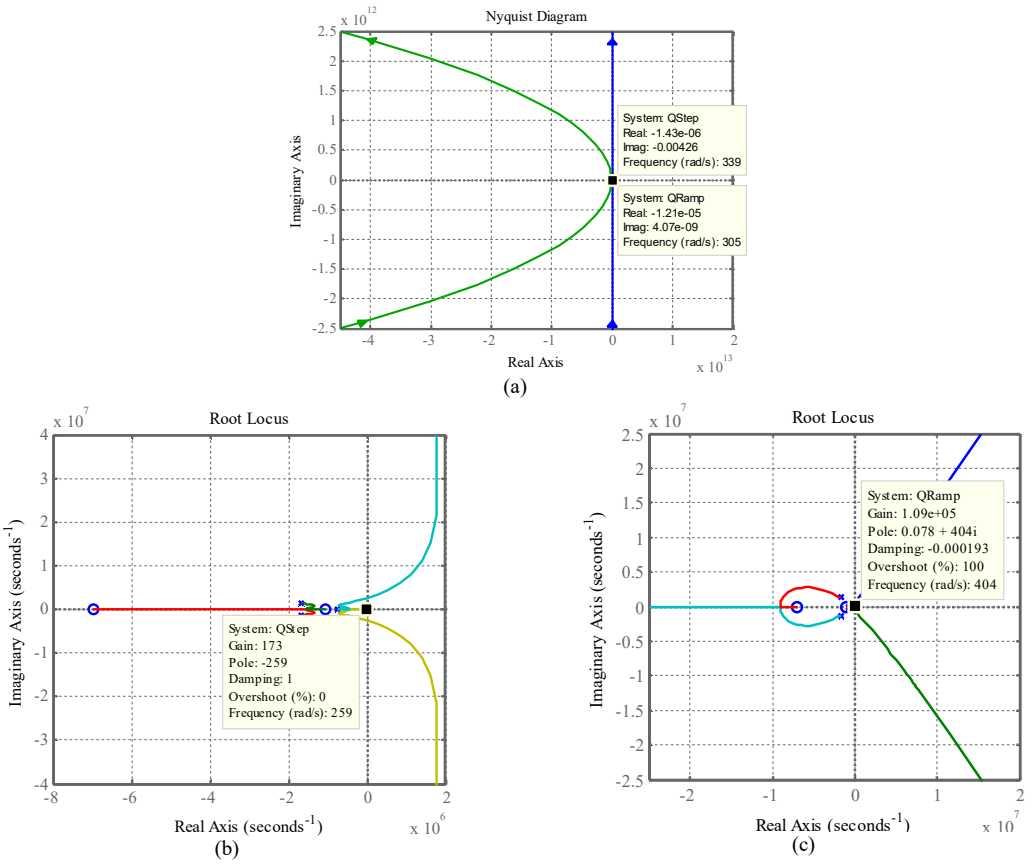

Fig. 8. VMPE effects on reactive power: (a) Nyquist diagram for step and ramp changes, (b) Root Locus diagram for step change, and (c) Root Locus diagram for ramp change.

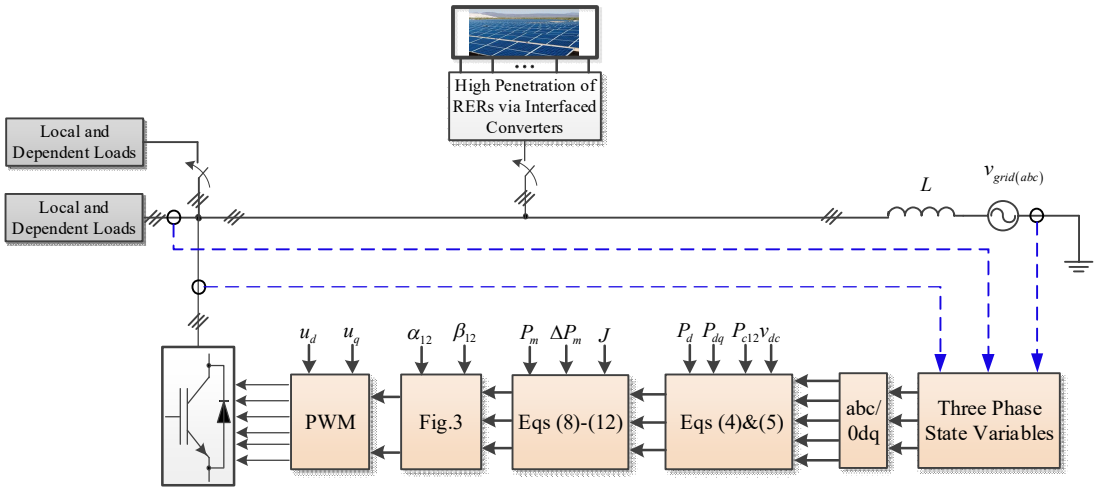

Fig.9. General structure of the proposed control technique.

A. Assessment of the Proposed Control Technique under Dynamic and Steady State Operating Conditions

The proposed control-based converter shown in Fig. 9 is intended to supply 3kW+j2kVAR load and then compensate an increment of 4kW+j3kVAR load at t=0.25s. Also, a high penetration of RERs into the power grid happens at t=0.1s. The active and reactive power of the interfaced converter and also the grid frequency and voltage magnitude in this scenario are illustrated in Fig. 10.

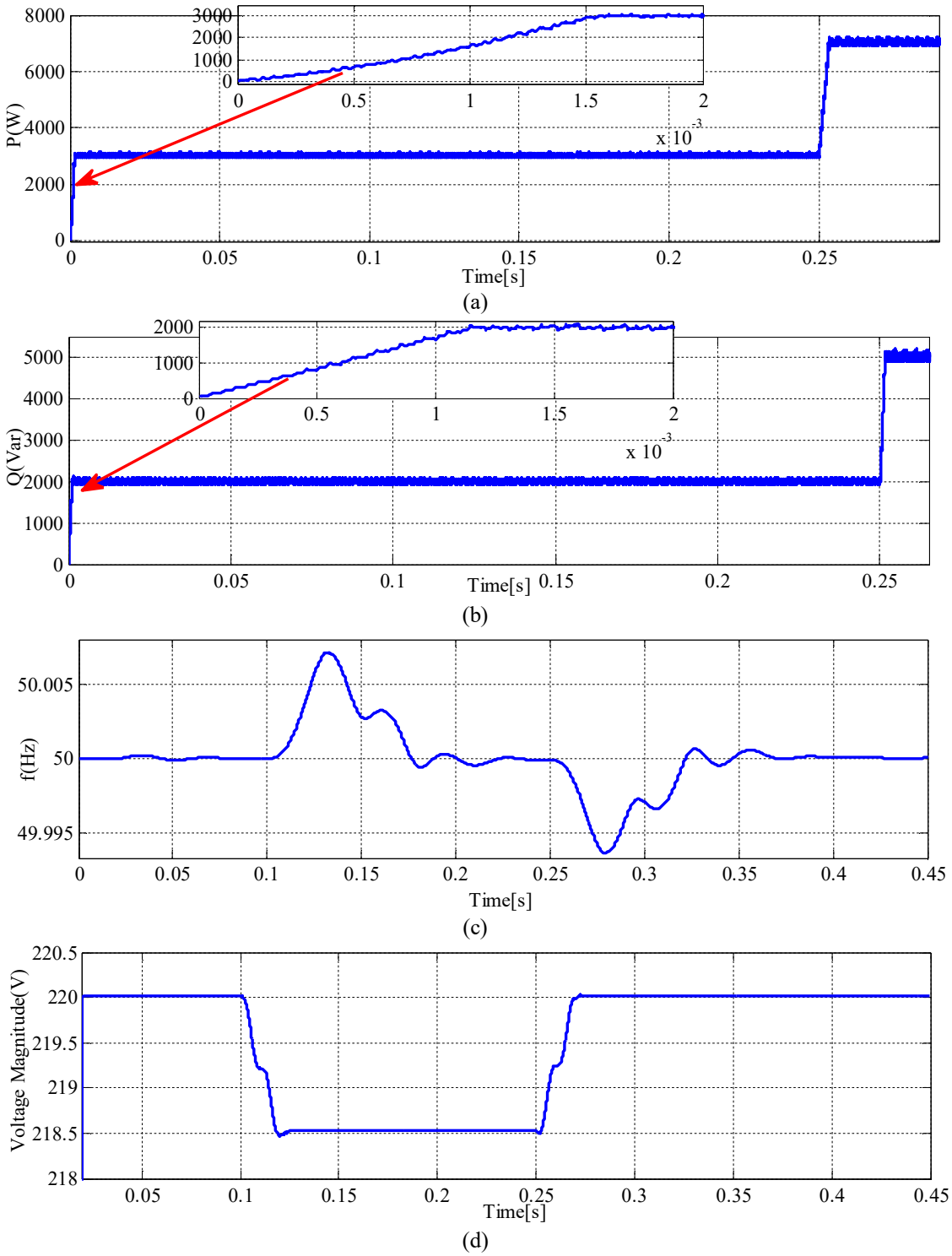

Fig.10. Operation of the proposed control technique under dynamic and steady state operating conditions: (a) active power, (b) reactive power, (c) the rid frequency, and (d) the grid voltage magnitude.

According to this figure, an accurate active and reactive power sharing can be performed by the proposed control-based converter with acceptable responses for both start point and dynamic change conditions. Also, fluctuations of the active and reactive power are negligible during tracking of their reference values.

On the other hand, according to Fig. 10(c), the grid frequency will reach its reference value with acceptable transient response after operation of the proposed control-based converter at t=0.25s. After high penetration of RERs into the power grid at t=0.1s, the grid voltage magnitude is fallen based on Fig. 10(d). As can be seen, the proposed control-based converter can appropriately force the grid voltage magnitude to achieve its desired value with acceptable dynamic response and by injecting the required active and reactive power at t=0.25s.

B. Impacts of Variations of VMPE and VI on the proposed control technique

This sub-section confirms that, the variations of VMPE and VI in the proposed control technique can impact on the grid frequency and voltage magnitude responses in both steady state and dynamic operating conditions. A high penetration of RERs at t=0.1 and its related compensation at t=0.25s will be occurred in this sub-section. Fig. 11 shows the grid frequency responses by changing VI and VMPE. It can be understood from Fig. 11(a) that very low and high values for VI will deteriorate both steady state and dynamic responses of the grid frequency. Only the middle values of VI will lead to acceptable response for the grid frequency. On the other hand, as depicted in Fig. 11(b), small VMPE can provide stable response for the grid frequency. It can be realized that, very high value for VMPE leads to a divergent response for the grid frequency. Fig. 12 shows the impacts of varied VI and VMPE on the grid voltage magnitude. According to Fig. 12(a), however the grid voltage magnitude response due to very low value of VI can follow its desired value after the proposed control-based converter compensation at t=0.25s, but the stable response cannot finally be achieved. For Fig. 12(a), the worst case belongs to very high VI. Similar to the grid frequency response, very good response for the grid voltage magnitude can be obtained by a low VMPE and very high values for VMPE can make an unstable response for the grid voltage magnitude as shown in Fig. 12(b).

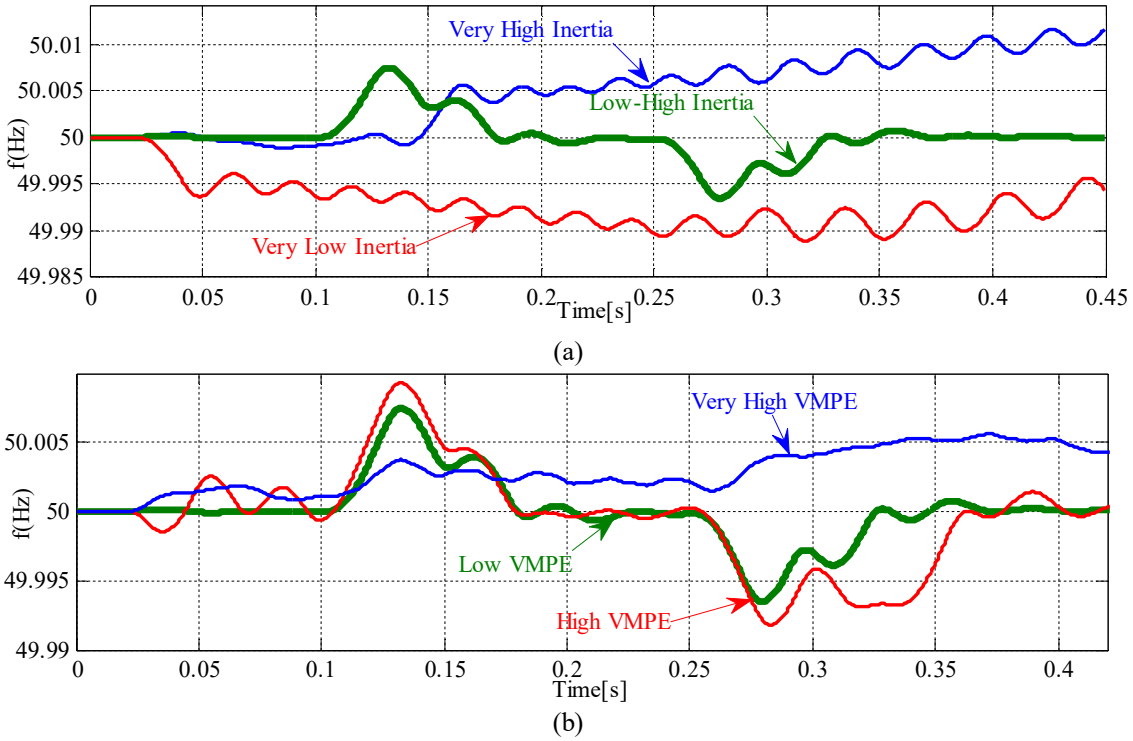

Fig.11. The grid frequency responses due to: (a) various VI, and (b) various VMPE.

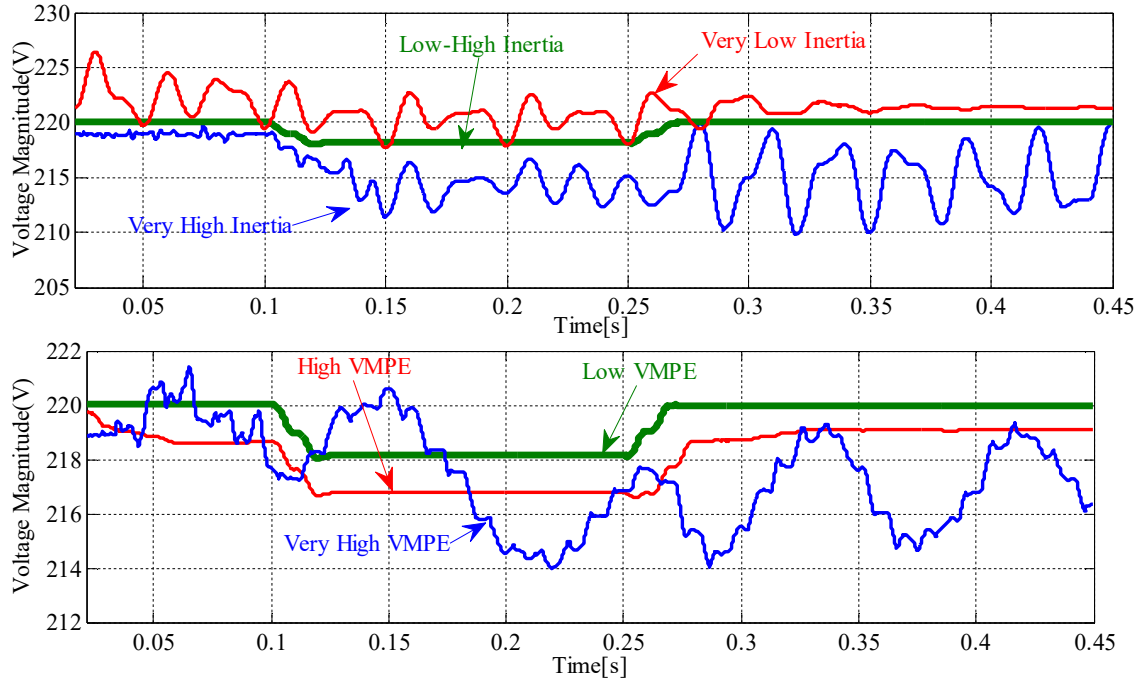

Fig. 12. Responses of the grid voltage magnitude due to: (a) various VI, and (b) various VMPE.

VII. Conclusion

A control technique has been presented in this paper for control of interfaced converters with high penetration of renewable energy resources into the power grid. The proposed control technique is based on inherent characteristics of SGs to guarantee a stable operation of the power grid. Key features of an SG i.e., virtual inertia, virtual mechanical power error, and reference value of virtual mechanical power have been included in the power-based dynamic model of the proposed model to emulate behaviour of SG in operation of interfaced converters. In fact, the proposed control technique presented a new model of power electronics-based SG to guarantees a stable operating condition for the power grid with high penetration of RERs, which has been considered as the main contribution of this work over the other existing works in this area. Two P-Q and P_m-Q curves have been extracted by use of the dynamic models of the proposed control technique and some related analyses have been involved for evaluation of the proposed control technique under different operating conditions. Moreover, VMPE and other error components variations have been considered for the evaluations of the grid frequency error through Nyquist diagrams for different VI values. The analysis of the proposed control technique based on the embedded SG inherent features has been completed by achieving two transfer functions in order to investigate the VMPE effects on the active and reactive power sharing of the interfaced converter in presence of different VI values.

Acknowledgment

J.P.S. Catalão acknowledges the support by FEDER funds through COMPETE 2020 and by Portuguese funds through FCT, under Projects SAICT-PAC/0004/2015 - POCI-01-0145-FEDER-016434, POCI-01-0145-FEDER-006961, UID/EEA/50014/2013, UID/CEC/50021/2013, UID/EMS/00151/2013, and 02/SAICT/2017 - POCI-01-0145-FEDER-029803, and also funding from the EU 7th Framework Programme FP7/2007-2013 under GA no. 309048.

References

[1] Xie L, Carvalho PMS, Ferreira LA, Liu J, Krogh BH, Popli N, Ilic MD. Wind integration in power systems: Operational challenges and possible solutions. Proceedings of the IEEE 2011; 99 (1): 214-232.

[2] Simoglou CK, Bakirtzis EA, Biskas PN, Bakirtzis AG. Optimal operation of insular electricity grids under high RES penetration. Renewable Energy 2016; 86: 1308-1316.

[3] Trivedi A, Singh M. Repetitive Controller for VSIs in Droop-Based AC-Microgrid. IEEE Transactions on Power Electronics 2017; 32 (8): 6595 – 6604.

[4] Mehrasa M, Pouresmaeil E, Mehrjerdi H, Jørgensen BN, Catalão JPS. Control technique for enhancing the stable operation of distributed generation units within a microgrid. Energy Conversion and Management 2015; 97: 362–373.

[5] Nasirian V, Shafiee Q, Guerrero JM, Lewis FL, Davoudi A. Droop-Free Distributed Control for AC Microgrids. IEEE Transactions on Power Electronics 2016; 31 (2): 1600 – 1617.

[6] Mehrasa M, Pouresmaeil E, Jørgensen BN, Catalão JPS. A control plan for the stable operation of microgrids during grid-connected and islanded modes. Electric Power Systems Research 2015; 129: 10-22.

[7] Karapanos V, Kotsampopoulos P, Hatziargyriou N. Performance of the linear and binary algorithm of virtual synchronous generators for the emulation of rotational inertia. Electric Power Systems Research 2015; 123: 119-127.

[8] Yang L, Wang J, Ma Y, Wang J, Zhang X, Tolbert LM, Wang FF, Tomsovic K. Three-Phase Power Converter-Based Real-Time Synchronous Generator Emulation. IEEE Transactions on Power Electronics 2017; 32 (2): 1651 – 1665.

[9] Bevrani H, Ise T, Miura Y. Virtual synchronous generators: A survey and new perspectives. International Journal of Electrical Power & Energy Systems 2014; 54: 244-254.

[10] Fang J, Tang Y, Li H, Li X. A Battery/Ultracapacitor Hybrid Energy Storage System for Implementing the Power Management of Virtual Synchronous Generators. IEEE Transactions on Power Electronics 2018; 33 (4); 2820 – 2824.

[11] D'Arco S, Suul JA, Fosso OB. A Virtual Synchronous Machine implementation for distributed control of power converters in Smart Grids. Electric Power Systems Research 2015; 122: 180-197.

[12] Nanou SI, Papakonstantinou AG, Papathanassiou SA. A generic model of two-stage grid-connected PV systems with primary frequency response and inertia emulation. Electric Power Systems Research Volume 2015; 127: 186-196.

[13] Liu J, Miura Y, Ise T. Comparison of Dynamic Characteristics between Virtual Synchronous Generator and Droop Control in Inverter-Based Distributed Generators. IEEE Transactions on Power Electronics 2016; 31 (5): 3600 – 3611.

[14] Huang L, Xin H, Wang Z, Wu K, Wang H, Hu J, Lu C. A Virtual Synchronous Control for Voltage-Source Converters Utilizing Dynamics of DC-Link Capacitor to Realize Self-Synchronization. IEEE Journal of Emerging and Selected Topics in Power Electronics 2017; 5(4):1565 – 1577.

[15] Zhu J, Guerrero JM, Hung W, Booth CD, Adam GP. Generic Inertia Emulation Controller for Multi-Terminal Voltage-Source-Converter High Voltage Direct Current Systems. IET Renewable Power Generation 2014; 8(7): 740 – 748.

[16] Pradhan C, Bhende CN, Samanta AK. Adaptive virtual inertia-based frequency regulation in wind power systems. Renewable Energy 2018; 115: 558-574.

[17] Fini MH, Golshan MEH. Determining optimal virtual inertia and frequency control parameters to preserve the frequency stability in islanded microgrids with high penetration of renewables. Electric Power Systems Research 2018; 154: 13-22.

[18] Alatrash H, Mensah A, Mark E, Haddad G, Enslin J. Generator Emulation Controls for Photovoltaic Inverters. IEEE Transactions on Smart Grid 2012; 3(2):996 – 1011.

[19] Aouini R, Marinescu B, Kilani KB, Elleuch M. Synchronverter-Based Emulation and Control of HVDC Transmission. IEEE Transactions on Power Systems 2016; 31(1): 278 – 286.